Published online 14 December 2006 *Nucleic Acids Research, 2007, Vol. 35, No. 2* ***441–454***
doi:10.1093/nar/gkl1066

L11 domain rearrangement upon binding to RNA and thiostrepton studied by NMR spectroscopy

Hendrik R. A. Jonker[1], Serge Ilin[1], S. Kaspar Grimm[1,2], Jens Wöhnert[1,2,*] and Harald Schwalbe[1,*]

[1]Johann Wolfgang Goethe-University, Institute for Organic Chemistry and Chemical Biology, Center for Biomolecular Magnetic Resonance, Max-von-Laue-Strasse 7, 60438 Frankfurt am Main, Germany and [2]University of Texas Health Science Center SA, Department of Biochemistry, 7703 Floyd Curl Drive, San Antonio, TX 78229, USA

Received October 11, 2006; Revised and Accepted November 20, 2006

ABSTRACT

Ribosomal proteins are assumed to stabilize specific RNA structures and promote compact folding of the large rRNA. The conformational dynamics of the protein between the bound and unbound state play an important role in the binding process. We have studied those dynamical changes in detail for the highly conserved complex between the ribosomal protein L11 and the GTPase region of 23S rRNA. The RNA domain is compactly folded into a well defined tertiary structure, which is further stabilized by the association with the C-terminal domain of the L11 protein ($L11_{ctd}$). In addition, the N-terminal domain of L11 ($L11_{ntd}$) is implicated in the binding of the natural thiazole antibiotic thiostrepton, which disrupts the elongation factor function. We have studied the conformation of the ribosomal protein and its dynamics by NMR in the unbound state, the RNA bound state and in the ternary complex with the RNA and thiostrepton. Our data reveal a rearrangement of the $L11_{ntd}$, placing it closer to the RNA after binding of thiostrepton, which may prevent binding of elongation factors. We propose a model for the ternary L11–RNA–thiostrepton complex that is additionally based on interaction data and conformational information of the L11 protein. The model is consistent with earlier findings and provides an explanation for the role of $L11_{ntd}$ in elongation factor binding.

INTRODUCTION

The ribosome is a large ribonucleoprotein complex that translates the genetic code from mRNA into a polypeptide chain during protein synthesis. Detailed structural information is presently known that reveals the two subunit complex structure of the RNA and the associated proteins, resulting in a wealth of information about protein–RNA interactions (1–6). Various Cryo-EM and X-ray structures are currently available of the ribosome trapped in different states of the translation process, including mRNAs, tRNAs, translation factors, release factors and antibiotics (7–21). Some regions in the molecular structure turned out to be rather flexible and at the same time are possible targets for antibiotics and are involved in regulation. Studies of these individual regions by high-resolution structural techniques largely contribute to understanding the dynamical properties and mechanisms of the proteins involved in ribosomal protein synthesis.

The complex between the ribosomal protein L11 and the 23S rRNA domain is an essential part (22,23) of the ribosomal GTPase-associated region (GAR). L11 is a highly conserved two-domain protein and has a specific role both in EF-G dependent GTP hydrolysis and in release factor 1 (RF-1) dependent termination (24,25). The C-terminal domain of L11 ($L11_{ctd}$) is primarily involved in binding to a well-conserved 58 nt sequence in the GAR region. This ribosomal RNA region shows a compact fold, which is stabilized by extensive tertiary contacts (26,27). An essential monovalent ion-binding-site must be occupied for the RNA to fold (28) and Mg^{2+}, which is essential under most conditions, can be replaced by high concentrations of monovalent ions (29,30). Biochemical experiments have shown that the RNA structure is further stabilized by the presence of $L11_{ctd}$ (31–33). The structures of full-length L11 and $L11_{ctd}$ in its free form have been solved by NMR (34–36). Moreover, the structure of L11 in complex with its cognate RNA has been characterized by NMR for $L11_{ctd}$ and solved by X-ray crystallography for $L11_{ctd}$ as well as full-length L11 (26,27,37). Cryo-EM and X-ray experiments show that the location of the N-terminal domain of L11 ($L11_{ntd}$) differs upon binding of EF-G (38), the release factors 1 and

*To whom correspondence should be addressed. Tel: +69 7982 9737; Fax: +69 7982 9515; Email: schwalbe@nmr.uni-frankfurt.de
*Correspondence may also be addressed to Jens Wöhnert. Tel: +1 210 567 3743; Fax: +1 210 567 6595; Email: jewoe@biochem.uthscsa.edu
Present address:
Serge Ilin, Sloan-Kettering Institute, Structural Biology Program, 1275 York Avenue, New York, NY 10021, USA

2 (19), EF-Tu, GDP and kirromycin (39), and with respect to an initiation-like state of the ribosome (17). Furthermore, recent X-ray structures of the ribosome (6) show additional orientations for $L11_{ntd}$. Altogether, these observations strongly suggest that the dynamical behavior of both L11 domains is important for its function during the ribosomal cycle. Since $L11_{ntd}$ makes only limited contacts to the RNA, this may allow interaction with the elongation and initiation factors.

Interestingly, the L11–RNA complex is targeted by the thiazole family of natural antibiotics such as thiostrepton and micrococcin (22,40,41). Thiostrepton is known to inhibit the EF-G function and the binding of release factors (42–44). Biochemical studies show that thiostrepton binds at the hairpin loop regions containing A1067 and A1095 (45–48) and may inhibit EF-G dependent translocation by hindering conformational changes in this region (49,50). Thiostrepton-resistant mutants of the L11 protein have been discovered that contain proline to serine or threonine mutations in the $L11_{ntd}$ (50,51). Furthermore, biochemical footprinting indicated that addition of thiostrepton induces a strong protection at the junction of both L11 domains, while the mutants were significantly less protected. Another study showed that all spontaneous thiostrepton-resistant mutations were found at conserved positions in the $L11_{ntd}$ or the RNA (52). Moreover, mutational analysis of several proline sites in $L11_{ntd}$ suggested that the resistance to thiostrepton may be caused by a more solvent-accessible conformation of this domain. A model has previously been proposed for the interaction of thiostrepton with the RNA that was based on NMR and methylation data of the RNA–thiostrepton binary complex (53). A limitation of this previous study is the absence of the L11 protein, although it has been implemented in the binding model using the X-ray structure of the L11–RNA complex (26). The affinity of thiostrepton to 23S rRNA is strongly enhanced by the presence of $L11_{ntd}$ (54,55). It appears that thiostrepton may block the conformational rearrangement of $L11_{ntd}$, therefore interfering with interaction of EF-G with the ribosome.

To get more insight into the role of L11 in the ribosome, we have investigated the conformational dynamics of L11 comprising both domains in its free form and in complex with either its cognate RNA region or both the RNA and thiostrepton. The dynamical properties and conformational transitions are studied by heteronuclear NMR relaxation measurements. The relative domain orientation is investigated for the binary L11–RNA and ternary L11–RNA–thiostrepton complex using NMR residual dipolar coupling (RDC) data. We have identified the interaction surfaces and show that the dynamical properties and the orientation of the L11 protein domains change upon binding to the RNA and the thiostrepton antibiotic, which is important for its function. We propose structural models for the ternary complex that are based on a docking approach [HADDOCK (56)] using NMR chemical shift data and RDCs for the L11 protein. The models are in agreement with NMR and biochemical results from others and additionally reveal the structural rearrangement of $L11_{ntd}$ in the complex.

MATERIALS AND METHODS

Sample preparation

The L11 protein (1–141 from *Thermotoga maritima*) was prepared essentially as described before (36). Labeled (^{15}N) protein was obtained by over-expression in *Escherichia coli* strain BL21(DE3) using 0.5 g/l $^{15}NH_4Cl$ (CIL) and 4.0 g/l ^{12}C-glucose in minimal media. Triple labeled ($^{2}D,^{15}N,^{13}C$) L11 was obtained using stable isotope labeled OD2 CDN media (Silantes).

The RNA fragment corresponds to 1050–1109 nt of *E.coli* 23S rRNA (57). The 60 nt RNA sequence (5′-GGGCAGGAUGUAGGCUUAGAAGCAGCCAUCAUUUAAAGAA AGCGUAAUAGCUCACUGCCC-3′) differs slightly from *E.coli* in the last four 3′ and 5′ nt and by a single base substitution, U1061A, to stabilize the tertiary structure (58). Unlabeled RNA was prepared by *in vitro* transcription with T7 RNA polymerase from linearized plasmid DNA templates (59). The unlabeled rNTPs were purchased from Sigma. The DNA template consisted of a T7 promoter region followed by the RNA coding sequence and a SmaI restriction site overlapping with the 3′ end of the coding sequence. The pUC19-plasmid containing the appropriate insert was amplified in *E.coli* strain DH5α and purified using a Qiagen-Mega purification kit. The plasmid was linearized with SmaI and subsequently purified. The *in vitro* transcription for production of the RNA was performed for 4 h at 37°C in 30 ml [200 mM Tris–Glutamic acid (pH 8.1), 20 mM 1,4-DTT, 2 mM spermidine, 40 mM $Mg(OAc)_2$, 5 mM of rNTP mixture, 50 μg/ml DNA template and 50 μg/ml T7 RNA polymerase]. The RNA was purified on a diethylaminoethyl (DEAE) sepharose fast flow column (APB) developed with a sodium acetate buffer step gradient (0–3 M, pH 5.5). The RNA in the selected fractions (denaturing PAA gels) was precipitated with 4× vol of ethanol overnight at −20°C. The air dried pellet (centrifugation in a Heraeus #7588 rotar for 30 min at 9000 *g*, 4°C) was dissolved in water to a concentration of 150 OD_{260}/ml and purified by high-performance liquid chromatography (HPLC) on a preparative C18 column (Vydac) with 50 mM potassium phosphate buffer (pH 5.9) and 2 mM tetrabutylammonium hydrogensulfate employing an acetonitrile gradient (60%). The RNA was freeze-dried, resuspended in water and desalted by repeated dilution and concentration using Centriprep 3K filters (Millipore). The final RNA was folded (monitored by native PAA gels) by heating to 95°C and cooling by 5× dilution with ice cold refolding buffer.

The thiostrepton from *Streptomyces azureus* was purchased from Sigma.

NMR spectroscopy

The NMR-samples were exchanged to a 20 mM potassium phosphate buffer (pH 6.1) containing 200 mM KCl, 5% D_2O, Complete Protease Inhibitor (Roche) and Superase-in RNase Inhibitor (Ambion), by repeated dilution and concentration using Centriprep 3K filters (Millipore). The protein concentration was ∼0.2–1 mM in all experiments. NMR experiments were performed at 298 K essentially as described in Cavanagh *et al.* (60) on Bruker 600, 800 and 900 MHz

spectrometers equipped with cryogenic triple-resonance probes. For the L11–RNA complex, little excess (1.5×) of the unlabeled RNA was added and no significant changes were observed anymore in the (^{1}H,^{15}N)-HSQC spectra after the last addition. The thiostrepton was added to a diluted L11 + RNA sample, containing 5% of dimethyl sulfoxide (DMSO). The sample was heated for 5 min at 70°C and exchanged towards NMR buffer by repeated dilution and concentration using Centriprep 3K filters (Millipore).

The spectrometer was locked on D_2O. Spectra were processed using the software package NMRPipe (61) and analyzed using SPARKY 3 (T. D. Goddard and D. G. Kneller, University of California, San Francisco). The resonances for the free form of L11 have been assigned before (62). Sequential backbone resonance assignment of labeled (^{2}D,^{15}N,^{13}C and ^{15}N) L11 in complex with unlabeled RNA (and thiostrepton) were obtained from a combination of triple resonance spectra, 3D HNCA, 3D HNCACB, 3D HNCO, overlaying the (^{1}H,^{15}N)-HSQC spectra of free L11 and L11 in complex and by verification of the NOE patterns from high-resolution 3D NOESY-(^{1}H,^{15}N)-HSQC spectra. RDCs were measured for the ^{2}D,^{15}N,^{13}C labeled L11 in complex samples in pf1 phage (16 g/l) alignment media (Profos) at 600 MHz. The ^{1}D(N,H) were extracted from IPAP-(^{1}H,^{15}N)-HSQC spectra (63,64). Signals that could be tracked reliably and determined unambiguously were analyzed using MODULE (65) and PALES (66). The ^{15}N relaxation experiments ({^{1}H}-^{15}N HetNOE, T_1 and T_2) (67–69) were performed for the ^{15}N labeled L11 in complex samples at 600 MHz. The longitudinal ^{15}N relaxation rates were determined from a series of spectra with delays of 100, 400, 800, 1200, 1600, 2000, 2800 and 3600 ms. Relaxation delays used for determining the transverse relaxation rates were 0, 17.6, 35.2, 52.8, 70.4, 88.0, 123.2 and 158.4 ms. The dynamics calculation using HetNOE values and T_1/T_2 ratios was performed using the TENSOR 2.0 program (70). The program performed a Lipari-Szabo type analysis (71,72) with 500 Monte-Carlo cycles for the internal mobility using the anisotropic diffusion tensor. The analysis has been repeated using the five best structures of each ensemble. The overall rotation correlation time τ_c was compared to the theoretical value estimated by hydrodynamic calculations performed by using the bead model of HydroNMR (73).

Structure calculation

Structures of L11 in complex with either RNA or RNA and thiostrepton were calculated using the simulated annealing (SA) protocol with torsian angle dynamics (TAD) implemented in CNS 1.1 (74) with the protein allhdg 5.3 force field (75). The structures were calculated based on the Cα distance restraints genererated using PERMOL (76), carbon Cα and Cβ chemical shift data and RDC data. The Cα distance restraints were derived from diverse PDB files containing L11 in complex with RNA: 1MMS, 487D, 1JQT, 1JQS, 1JQM, 1R2W, 1R2X, 2B9P, 1NKW, 1PNU, 1SM1, 2AW4, 2AWB, 1P85 and 1P86 using the low- and high-values for each restraint up to a maximum distance of 20 Å. Accordingly, these Cα distance restraints define the optimal local geometry and at the same time allow for all possible L11 domain orientations. The axial (Da) and rhombic (Dr) components of the alignment tensor were estimated using PALES (66). The final values for Da and Dr were 7.8 and 0.3 for the L11–RNA complex and 6.0 and 0.5 for the L11–RNA–thiostrepton complex. The bond length of the pseudo-atoms of the alignment tensor was set to 10 Å to decrease the overall energy and to increase the convergence rate (77). The best 20 structures were selected based on pairwise backbone RMSD of the 40 lowest energy structures from 80 calculated structures.

Modelling of the L11–RNA–thiostrepton complex was achieved using a high ambiguity driven docking (HADDOCK) approach essentially as described by Dominguez *et al*. (56). We have used the HADDOCK2.0_devel software version in which the multi-component docking feature has been implemented. The ambiguous interaction restraints (AIRs) have been defined for the residues that exhibited significant chemical shift changes upon interaction with RNA and thiostrepton. Furthermore AIRs have been defined as indicated by Lentzen *et al*. (53). The dockings were performed using the RNA from the crystal structure of the L11–RNA complex [pdb:1MMS] (26), the thiostrepton crystal structure [pdb:1E9W] (78) and a bundle of the 20 best L11 structures, optimized using the RDCs for the L11–RNA–thiostrepton complex. The protein allhdg 5.3 force field (75) was used for the L11 and the dna-rna-allatom force field (79) for the RNA. The topology and parameter files for thiostrepton were generated using the PRODRG server (80). The 200 final water-refined docking results are clustered at the interface within a threshold of 4.0 Å pairwise backbone RMSD. The top-ranked ensemble, according to the average interaction energy and buried surface area, was accepted as the best representative of the complex.

RESULTS

Previous studies indicated different possible orientations for the two domains of L11 (6,17,19,38,39), which led us to investigate the dynamics and domain arrangements of this protein in its free form in comparison with the binary complex with its cognate RNA and with the ternary complex with the RNA and the thiostrepton antibiotic (Figure 1A). This is a challenging system to study by NMR, seen the diverse composition of the biomolecular system and the relative large size of the complex (36.1 kDa; L11: 15.1 kDa, RNA: 19.3 kDa and thiostrepton: 1.7 kDa).

Identification of the L11 interaction surfaces for RNA and thiostrepton

The ^{1}H, ^{15}N and ^{13}C backbone and side-chain resonances of the full-length L11 protein in its free form have been assigned and previously reported (62). The backbone assignment could be obtained with the exception of M1, A2, P22 and P73. Binding of L11 to the RNA was shown to be strongly dependent on the Mg^{2+} concentration as it is necessary for folding the RNA into its correct tertiary structure (58). However, upon titration of L11 with RNA in a buffer containing 5 mM Mg^{2+}, the ^{1}H^{15}N HSQC spectrum of the protein shows a significant line broadening with only ~60% of the expected signals distinguishable (data not shown). As a high concentration of potassium ions may substitute the

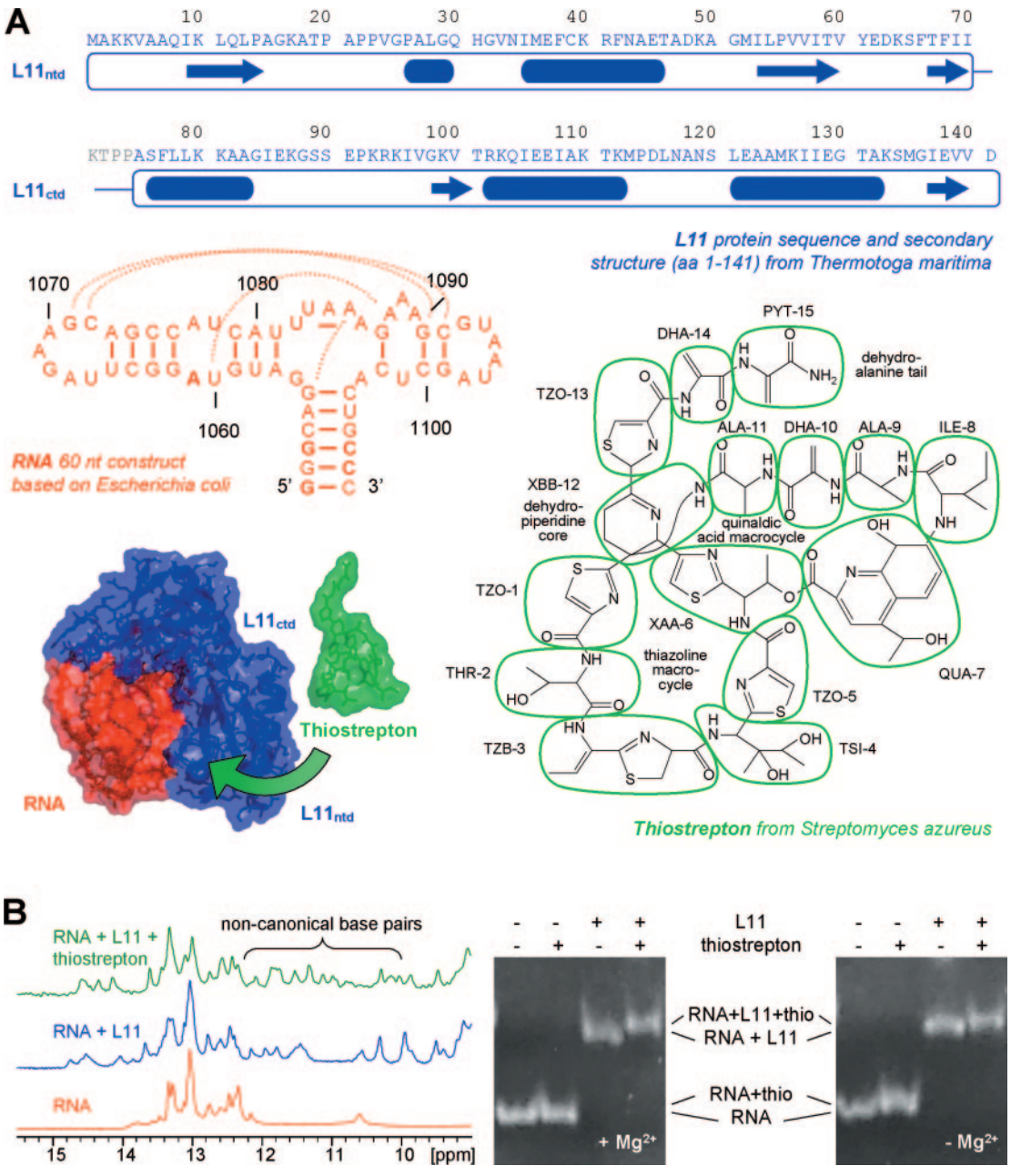

Figure 1. (**A**) The L11, RNA and thiostrepton components of the system showing the sequences and structures (26,78) of the three components. The L11 protein is indicated in blue, the 23S RNA region in red and the thiostrepton antibiotic in green. The sequence and secondary structure of the L11 protein is shown on top. Below are the secondary structure diagram of the RNA construct used (mutations in respect to the *E.coli* sequence indicated in bold) and a schematic structure of the thiostrepton antibiotic in which the 'residues' are indicated. (**B**) 1D ^{1}H NMR spectra of the RNA imino region in 200 mM KCl and native gel-shift assays of the RNA in presence and absence of Mg^{2+} in 200 mM KCl. The conditions are indicated above the lanes: with (+) or without (−) an excess of the L11 protein and thiostrepton antibiotic.

magnesium in the native RNA structure formation (28–30), the L11-binding was investigated by a gel-shift assay in the presence of 200 mM KCl (Figure 1B). As evident from this native gel, a stable homogenous RNA–protein complex formed in the absence of magnesium with a gel-shift very similar to the one with magnesium. This effect was confirmed by the observation of non-canonical base pair signals in the imino region of the ^{1}H 1D NMR spectrum of the RNA–L11 complex in 200 mM KCl (Figure 1B). Both observations show the complex formation which indicates that the RNA is properly folded (33,81). To determine the L11 regions involved in the interaction with RNA, a titration experiment was performed using triple labeled (^{2}D^{15}N^{13}C) L11 protein with unlabeled RNA. Upon addition of increasing amounts of RNA, many amide resonances of L11 in the ^{1}H,^{15}N correlation spectra disappeared and reappeared at a different chemical shift location. This observation is indicative for slow exchange between free and RNA bound form of L11 on the NMR time scale and characteristic for a high-affinity complex. As the chemical shift changes could not be

unambiguously mapped by stepwise titration of RNA to the protein due to the slow exchange, the amide resonances of the complex have been assigned. The chemical shift values have been deposited in the Biological Magnetic Resonance data Bank (BMRB, accession no. 7307). An overlay of the $^{1}H^{15}N$ TROSY-HSQC spectra of free L11 and the L11–RNA complex is shown in Figure 2A.

Since thiostrepton is poorly soluble in water, for preparation of the ternary L11–RNA–thiostrepton complex, the binary L11–RNA complex was diluted to a concentration of 10–30 μM with NMR buffer containing 5% DMSO. The structure of the complex was not affected by addition of DMSO as no chemical shift changes were observed in the $^{1}H,^{15}N$ correlation spectra (data not shown). An excess of the thiostrepton antibiotic was added and the sample was heated for 5 min at 70°C to enhance the solubility of thiostrepton and aid the binding if conformational and/or structural rearrangements of the L11-RNA would be needed. However, NMR data indicated that the complex was also formed without this heating step, indicating that no large scale refolding events need to occur for the RNA to bind to thiostrepton. Subsequently, the sample was exchanged and concentrated to NMR buffer without DMSO. The chemical shift changes observed upon binding to thiostrepton were significantly smaller (Figure 2B) with respect to the shifts observed upon binding to the RNA, indicating less dramatic structural changes. The amide resonances for the ternary complex could easily be re-assigned from the spectrum of the RNA–protein complex and have been verified using triple resonance spectra. The chemical shift values have been deposited in the BMRB (accession no. 7308).

As observable from the mapping of the chemical shift perturbations (CSPs) on the L11 sequence (Figure 3), the RNA-binding surface is located in the $L11_{ctd}$, which is in good agreement with the X-ray structure of the complex (26). The loop region (residues 86–96) and nearby residues are mostly effected upon the interaction. However, there are no considerable CSPs in $L11_{ntd}$, whereas the X-ray structure (26) of the complex suggests possible interactions between the RNA and $L11_{ntd}$ (residues 10–12, 30, 31 and 71). The 10–12 region in $L11_{ntd}$, which is closely located to the $L11_{ctd}$, shows relatively the largest perturbations. These moderate CSPs can either be caused by binding of this region to the RNA and by conformational changes in the protein when the $L11_{ctd}$ moves towards these residues of $L11_{ntd}$. Although the interactions may not necessarily have been translated to large amide chemical shift changes, our NMR findings indicate that the interactions between the $L11_{ntd}$ and the RNA in the X-ray structure may probably be due to crystal packing, in agreement with the different possible orientations of the N-terminal domain found in other X-ray structures that include L11 and its cognate RNA. Addition of thiostrepton to the L11–RNA complex mainly induced CSPs in the $L11_{ntd}$, which confirms the thiostrepton binding site as indicated by Lentzen *et al*. (53).

Analysis of L11 structures

Various X-ray and cryo-EM structures containing L11 and its cognate RNA are currently deposited in the protein Data Bank (PDB), showing different orientations for the L11 protein. In order to verify the relative domain orientation and its flexibility, the available full-length L11 structures were analyzed. Only the Cα traces have been compared as these are frequently the only coordinates deposited. For several PDB files, the Cα coordinates for the L11 protein are relatively the same as others; most often the ones first deposited in 1MMS by Wimberly *et al*. (26) are used and were thus not further taken into account. Dissimilar structural coordinates for the L11–RNA complex have been deposited for *T.maritima*: 487D (82), 1JQT & 1JQS & 1JQM (38), 1R2W & 1R2X (39), 2B9P & 2B66 & 2B9N (19), *Deinococcus radiodurans*: 1LNR & 1NKW (5), 1NWX & 1NWY (83), 1SM1 (84), 1PNU & 1PNY (85), 1VOR (86) and *E.coli*: 2AW4 & 2AWB (6), 1P85 & 1P86 (17). The Cα coordinates have been extracted and converted to the *T.maritima* sequence for L11 residues 8–140 before the pairwise root-mean-square deviation (RMSD) analysis (Supplementary Table 1). An overlay of all the different X-ray and cryo-EM structures of L11 is given in Figure 4A to indicate the conformational space that can be occupied by the two domains. The average RMSD to the mean for the stable secondary structure elements is rather small for the independent L11 domains (0.76 Å and 1.13 Å for either $L11_{ntd}$ and $L11_{ctd}$) but becomes much larger for the full-length protein (2.39 Å). A similar analysis has been performed for the PDB structures containing different orientations of both the L11 protein and its cognate RNA (Figure 4B). The average RMSD to mean for the RNA is 1.67 Å and 1.71 Å for both the RNA and $L11_{ctd}$ indicating only very little differences in the position of $L11_{ctd}$ relative to the RNA.

Dynamics of the ribosomal L11 protein

To investigate the effect of the structural rearrangement of the L11 domains on the dynamical properties of the protein, heteronuclear ^{15}N relaxation experiments ($\{^{1}H\}$-^{15}N HetNOE, T_1 and T_2 measurements) have been performed (Figure 5). Analysis of the relaxation data for the free L11 protein confirmed (36) that the two domains tumble together mostly in a rigid state as the overall rotational correlation time (τ_c) calculated for the whole protein (8.38 ± 0.03 ns) and the separate domains ($L11_{ntd}$: 7.90 ± 0.09 ns; $L11_{ctd}$: 8.65 ± 0.11 ns) are highly similar to each other and in the range of the value (10.2 ns) predicted by HydroNMR (73) and are clearly off the range for independently tumbling domains (4.2 ns). The τ_c value increases upon interaction with RNA (17.2 ± 0.4 ns; $L11_{ntd}$: 15.9 ± 0.4 ns; $L11_{ctd}$: 18.6 ± 0.4 ns) and further after addition of thiostrepton (18.5 ± 0.4 ns; $L11_{ntd}$: 16.7 ± 1.4 ns; $L11_{ctd}$: 19.0 ± 0.5 ns), which is close to the predicted value for the L11–RNA complex (18.7 ns). The presence of the flexible loop region in $L11_{ctd}$ (residues 86–96) for the free form of the protein is indicated by notably large HetNOEs, large T_2 values and low order parameters (S^2). When the protein is in complex with the RNA, the HetNOE and T_2 relaxation data and S^2 indicate a rigidification of this loop region to the same extent as the remainder of $L11_{ctd}$. This is well in agreement with the observed large CSPs in this region (Figure 3). When excluding the loop region, there is a slight variation in the T_2 relaxation ($L11_{ntd}$: 89 ± 1 ms; $L11_{ctd}$: 77 ± 1 ms) and T_1/T_2 ($L11_{ntd}$: 7.7 ± 0.2; $L11_{ctd}$: 8.9 ± 0.2) values which correlates to small

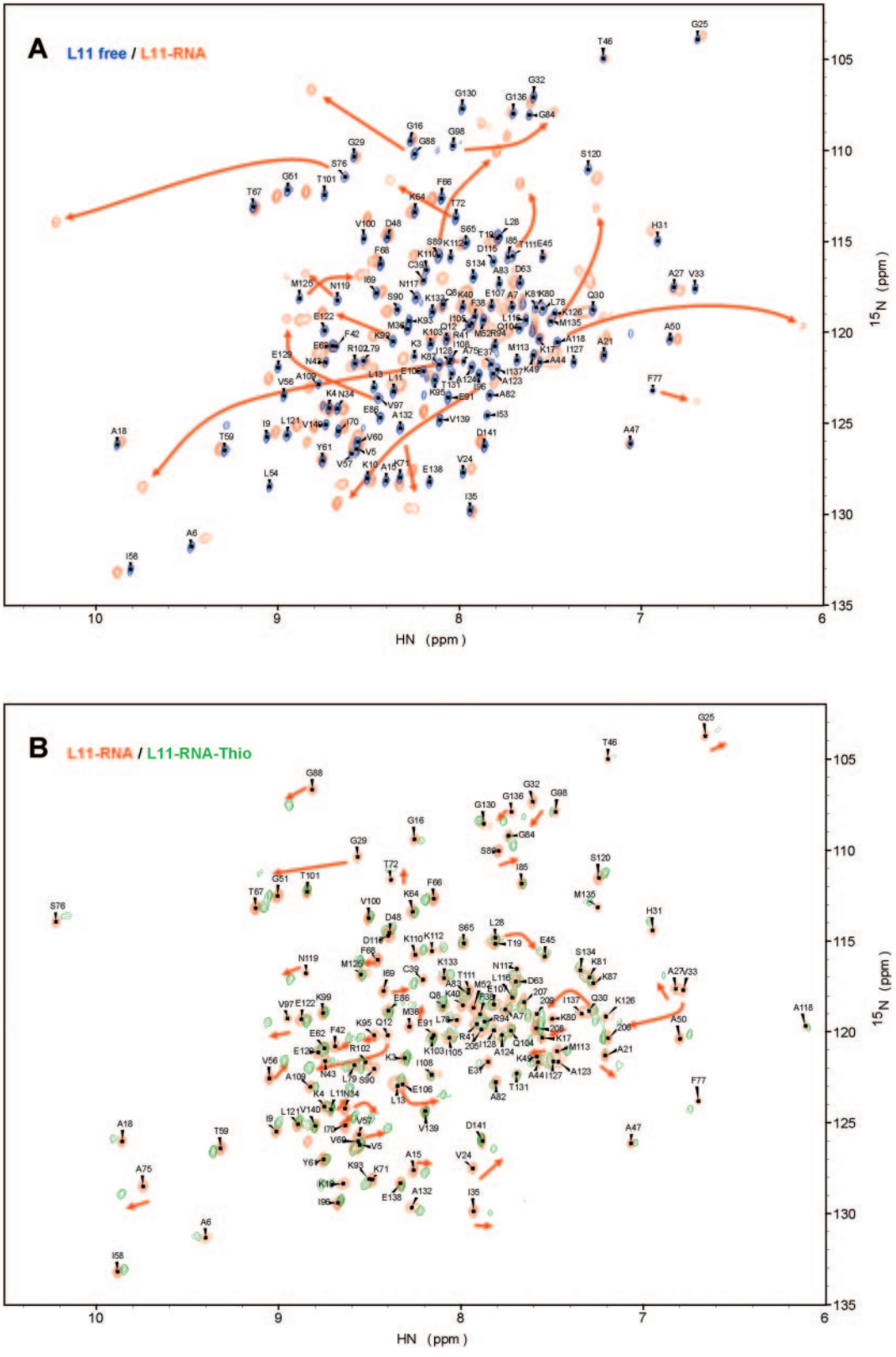

Figure 2. Overlay of the $^{1}H^{15}N$ TROSY-HSQC spectra (600 MHz) of L11 in its free form with the RNA bound form (**A**) and of L11 in the RNA bound form with the RNA and thiostrepton bound form (**B**). The backbone assignments for L11 are shown for its free form (A) and RNA bound form (B) and some of the major peak shifts are indicated by arrows. The spectra were aquired at 298 K in the same buffer solution [20 mM potassium phosphate buffer (pH 6.1), 200 mM KCl and 5% D_2O].

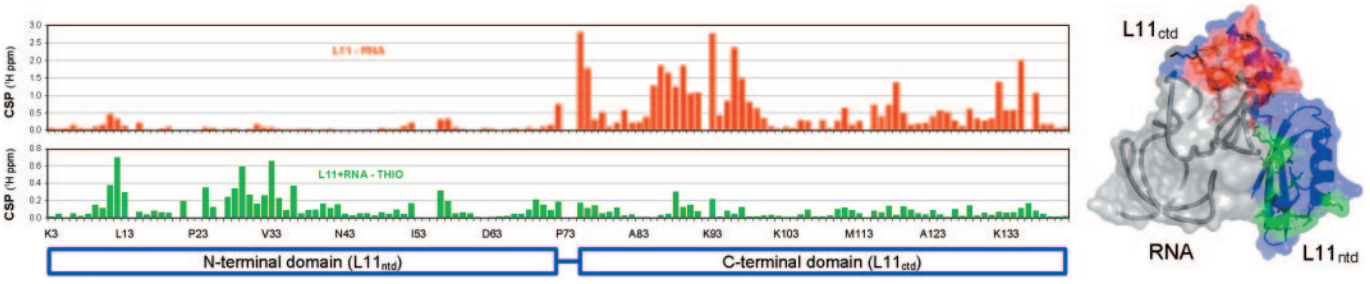

Figure 3. CSPs in L11 due to addition of RNA (red) and thiostrepton (green). The amide ^{1}H and ^{15}N resonance shifts have been mapped and combined as Euclidian distances between peak maxima taking into account the gyromagnetic ratio of proton and nitrogen (in ^{1}H p.p.m.). Missing bars indicate prolines or amide resonances that have not been assigned or could not be traced back for L11 in complex. The L11 interaction sites are indicated in red for the RNA (>1.0 p.p.m.) and green for thiostrepton (>0.3 p.p.m.) on the combined ribbon/surface representation of the L11–RNA complex (26) on the right.

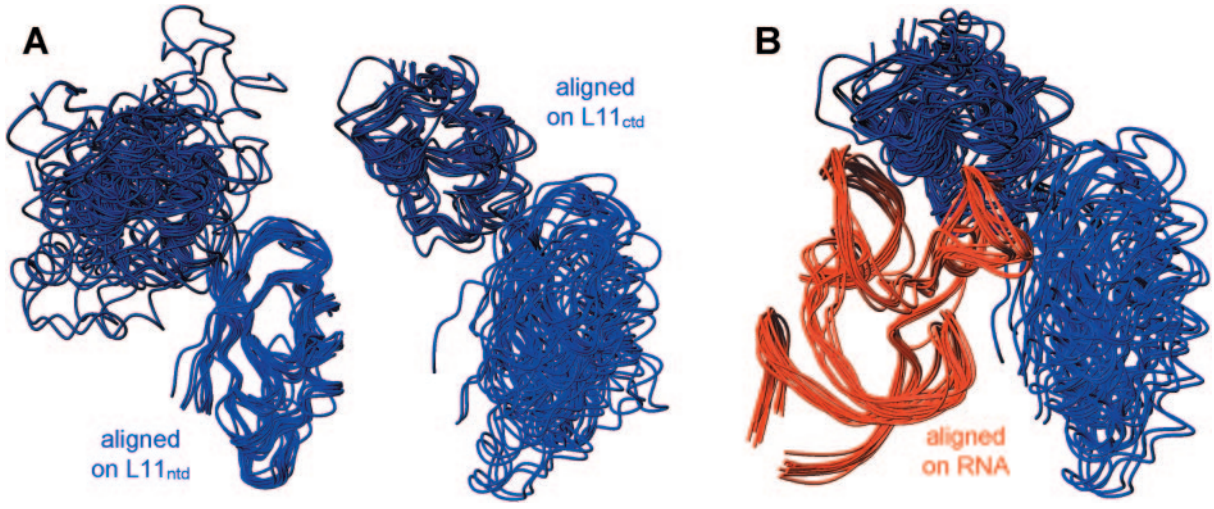

Figure 4. (**A**) Overlay of different X-ray and cryo-EM structures of the L11 protein. Cα traces have been extracted from the PDB files: 1MMS, 487D, 1JQT, 1JQS, 1JQM, 1R2W, 1R2X, 2B9P, 2B66, 2B9N, 1NKW, 1PNU, 1SM1, 1VOR, 2AW4, 2AWB, 1P85 and 1P86. The structures are aligned on the stable secondary structure elements of either the N-terminal domain ($L11_{ntd}$ in blue; residues 9–14, 26–29, 35–45, 53–59 and 67–69) or the C-terminal domain ($L11_{ctd}$ in dark blue; residues 76–83, 98–100, 102–112, 121–132 and 137–139). (**B**) Overlay of different X-ray and cryo-EM structures containing the L11 protein and its cognate RNA. Cα traces of L11 (blue) and P traces of the RNA (red) have been extracted from the PDB files: 1MMS, 1R2W, 1R2X, 2B9P, 2B66, 2B9N, 1NKW, 1NWX, 1NWY, 1PNU, 1PNY, 1LNR, 1SM1, 1VOR, 2AW4, 2AWB, 1P85 and 1P86. The structures are aligned on the RNA (1052–1108 nt).

differences in the τ_c values for both domains. The T_1 relaxation data indicate similar properties for both L11 domains in its free form since the average T_1 values for $L11_{ctd}$ and $L11_{ntd}$ are the same (670 ± 15 ms). Upon binding to the RNA, however, the T_1 relaxation data indicate that the overall tumbling motion of $L11_{ctd}$ (1290 ± 90 ms) decreases more than for $L11_{ntd}$ (1090 ± 45 ms). This is also apparent from the calculated T_1/T_2 ($L11_{ntd}$: 31 ± 5; $L11_{ctd}$: 39 ± 8) values for the L11–RNA complex and well in agreement with our notion of no significant CSPs in $L11_{ntd}$ (Figure 3) and the presence of multiple possible conformations (Figure 4). Interestingly, a further reduction in the overall tumbling motion is observed after binding of the thiostrepton antibiotic in which both L11 domains obtain similar dynamical properties again (T_1: 1450 ± 130 ms). For the ternary complex, there is only little deviation in the T_2 relaxation ($L11_{ntd}$: 43 ± 5 ms; $L11_{ctd}$: 38 ± 3 ms) and T_1/T_2 ($L11_{ntd}$: 37 ± 6; $L11_{ctd}$: 39 ± 4) values. Apparently, the antibiotic thiostrepton locks the $L11_{ntd}$ conformation in a more rigid (inhibitory) state that stabilizes the ternary L11–RNA–thiostrepton complex.

Determining the L11 domain orientation using RDCs

In order to determine the relative orientation of the L11 domains when in complex with RNA (and thiostrepton), RDCs were measured of L11 using pf1 phage alignment media. The phages did not disturb or interact with the L11 complexes as no chemical shift changes were observed in the ^{1}H, ^{15}N correlation spectra (data not shown). RDCs could be determined for many sites that were well distributed across both L11 domains. For the binary L11–RNA complex, 127 $^{1}D(N,H)$ have been measured and for the ternary L11–RNA–thiostrepton complex, 120 $^{1}D(N,H)$ have been measured. Other RDCs have been measured, but could not be determined reliably due to the large line-widths and/or the low signal to noise ratio. The RDC values have been deposited in the BMRB (accession nos 7307 and 7308). A direct comparison of the RDC data with the available X-ray structures is not very accurate as these structures frequently only contain a Cα trace and do not contain hydrogens. Therefore, we have calculated the L11 structures for the complexes using Cα distance restraints derived from the analyzed PDB

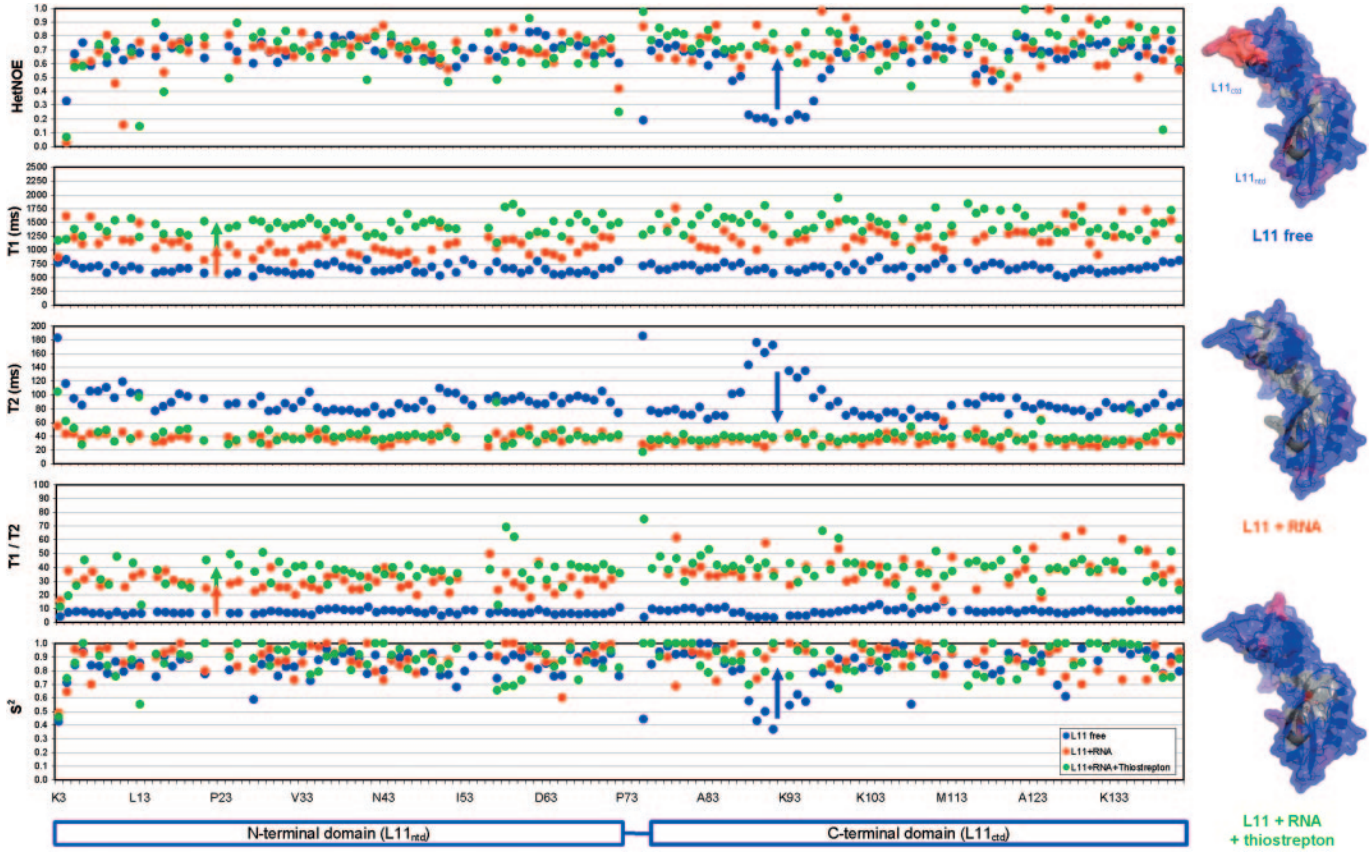

Figure 5. Internal dynamics of L11. Heteronuclear relaxation rates ({^{1}H}-^{15}N HetNOE, T_1 and T_2), T_1/T_2 ratios and the order parameters (S^2) of the backbone amides of L11 in its free form (blue), in complex with RNA (red) and in complex with RNA and thiostrepton (green). Missing bars indicate prolines or amide resonances that have not been (unambiguously) assigned or relaxation values that could not be determined reliable. The order parameter is indicated on the surface of the structures on the right [from blue (rigid, >0.9) to red (flexible, <0.55)]. The experiments were performed at 298 K in the same buffer solution [20 mM potassium phosphate buffer (pH 6.1), 200 mM KCl, 5% D_2O) at a field strength of 14.1 Tesla (600 MHz)].

files of L11 in combination with chemical shift data and the measured RDCs. The use of Cα distance restraints derived from the different X-ray structures additionally implements the 'flexibility' in the structure similar to the NOE data, and is therefore better than fitting the RDC data onto single X-ray structures. The structures have been calculated using NOEs and RDCs for free L11 (36) and Cα distance restraints and RDCs for the L11–RNA–(thiostrepton) complexes. Since our NMR data indicate that no considerable structural changes occur in the L11 protein after binding of the antibiotic and the RDC data fit well to both domains, the use of Cα distance restraints from the binary complex is justified. Both the NOEs and Cα distance restraints maintain the local structure of each domain, not the orientation. The RDCs are used in the same way for each calculation and determine the orientation of the domains. The back-calculated RDC values agree very well with the structures ($R = 0.98$). The structure of L11 when free in solution (36) has been compared to the calculated structures of L11 in complex (Figure 6). Apparently, a rearrangement occurs upon binding to the RNA and thiostrepton, placing the N-terminal domain of L11 closer to the RNA. Upon binding of L11 to the RNA, the first principal axis of the mass tensor of $L11_{ntd}$ turns 21 ± 2°, but the relative angle between the principal axis of both domains remains more or less the same (2 ± 2°). A further motion occurs after binding to thiostrepton when the first principal axis of $L11_{ntd}$ turns 26 ± 2° as compared to the RNA bound form. This rearrangement is mostly relative to the $L11_{ctd}$ as the angle between the principal axes of both domains also changes 24 ± 2°. When comparing the relative orientations of both domains with the analyzed structures form the PDB, the RNA bound orientation is most similar to the EF-G and EF-Tu bound structures [1JQM (38) and 1R2W (39)] although slightly rotated around the first principal axis of $L11_{ntd}$. The orientation for the ternary complex most closely resembles the orientation as found in the 2AWB (6) *E.coli* ribosome structure.

Docking of the ternary L11–RNA–thiostrepton complex

In order to more clearly understand the binding mode of thiostrepton to RNA and L11, a model for the ternary L11–RNA–thiostrepton structure (53) was calculated using HADDOCK (56) and improved by adding conformational information and interaction restraints for the L11 protein. In a first docking approach, the binding pocket for thiostrepton on the RNA was not pre-defined. The NOE based restraints between thiostrepton and the RNA (53) were incorporated in a highly ambiguous manner allowing interaction of thiostrepton with all possible adenine and cytosine residues

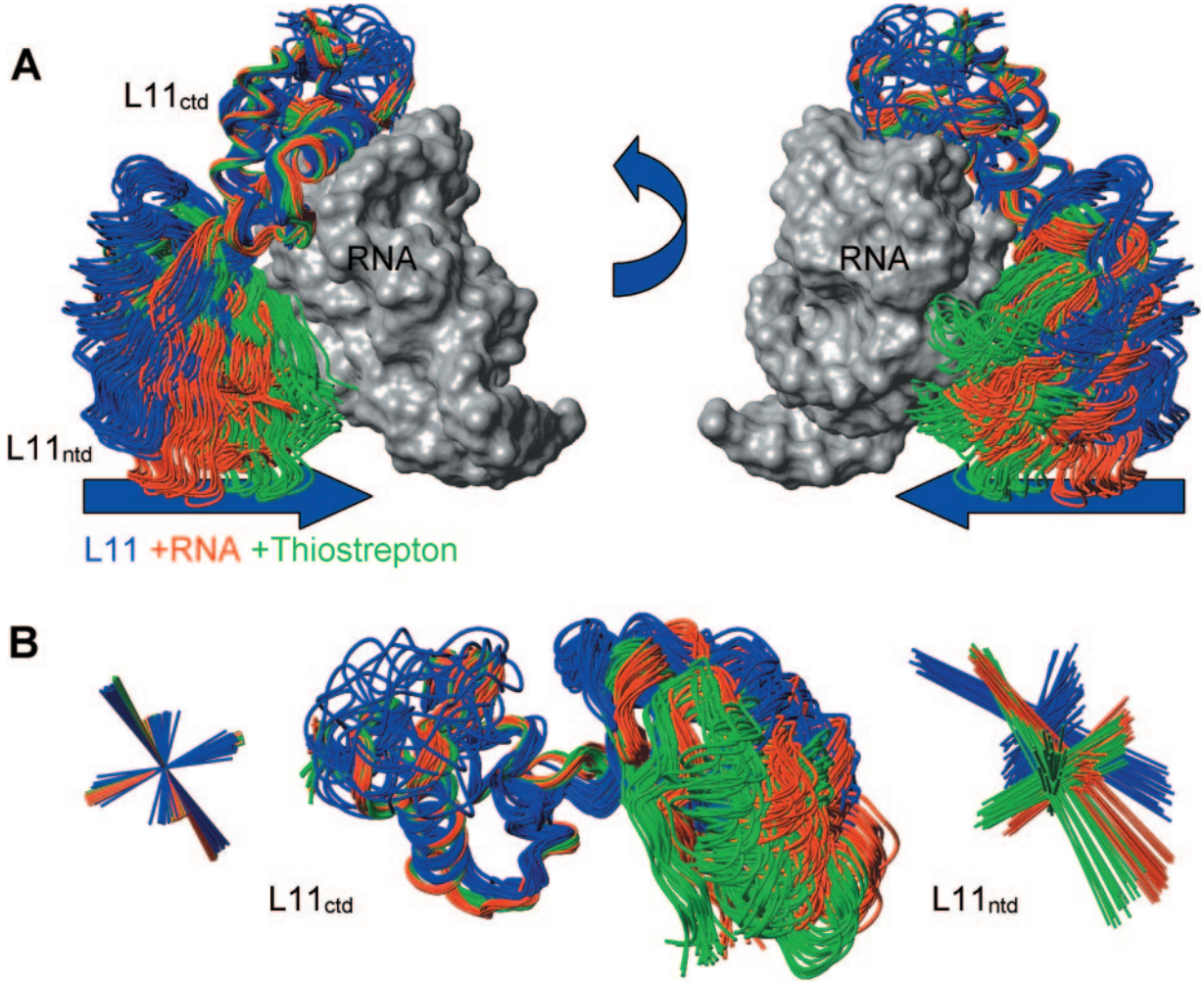

Figure 6. L11 domain orientations as determined using RDCs. Overlay of L11 structures calculated for the protein in its free form (blue), in complex with RNA (red) and in complex with RNA and thiostrepton (green). Every orientation is presented by a bundle of the 20 best structures shown as backbone trace. The free form L11 structure was calculated using NOE and RDC data as shown before (36). The structures for L11 in complex with RNA or RNA and thiostrepton were calculated by SA using Cα distance restraints from different X-ray L11 structures and measured RDCs. The structures are aligned on the stable secondary structure elements of $L11_{ctd}$ (residues 76–83, 98–100, 102–112, 121–132 and 137–139). The figures on the upper panel (**A**) include the van der Waals surface representation for the RNA that has been included by alignment of the X-ray structure of the L11–RNA complex (26). The figures on the lower panel (**B**) show a different orientation of the bundle and the calculated principal axis of the mass tensor.

of the RNA. Yet, the final lowest energy structures of the docking presented the binding pocket indeed to be at the RNA stem–loops containing A1067 and A1095. In further calculations, these restraints were incorporated to be fulfilled from the defined protons of thiostrepton to the defined protons of any adenosine and cytosine within or close to the binding pocket in order to avoid too much ambiguity and to increase the convergence rate. In the final calculation, all three components (L11, RNA and thiostrepton) were docked together. Both RNAs present in the X-ray structure from Wimberly *et al*. (26) were used as input. The 1D ^{1}H NMR spectra of the imino region of the RNA (Figure 1B) indicates some changes after binding of thiostrepton, which may be caused by conformational changes caused by binding of the thiostrepton to the RNA loop regions. Therefore, the side-chains in and near the binding interface (1057–1088 and 1094–1098 nt) for L11 and thiostrepton were left flexible during the semi-rigid docking. The thiostrepton X-ray structure of Bond *et al*. (78) was used, leaving the whole molecule flexible during all stages of the SA protocol. For the L11 protein, the bundle of 20 best structures as calculated with the RDCs from L11 in the ternary complex was used as input for the docking, leaving the side-chains flexible. AIRs between the RNA and thiostrepton were defined as derived from NMR (53) and mutational analysis (47). AIRs for the interactions between L11 and either the RNA or thiostrepton were based on the CSP data (Figure 3). As the observed chemical shift changes from thiostrepton binding could either be caused by thiostrepton and/or rearrangement of the L11 with respect to the RNA, this was left ambiguous.

The top-ranked docking model for the L11–RNA–thiostrepton complex (Figure 7A) shows the preferential binding orientation of the antibiotic to the RNA and protein. The final structures have been analyzed whether they satisfy the biochemical and structural restraints. The long polypeptide dehydroalanine chain of thiostrepton (Figure 1A) is positioned at the bottom of $L11_{ntd}$ (confirmed by CSPs of residues 29,33,36) and the thiazoline-macrocycle is located next to the

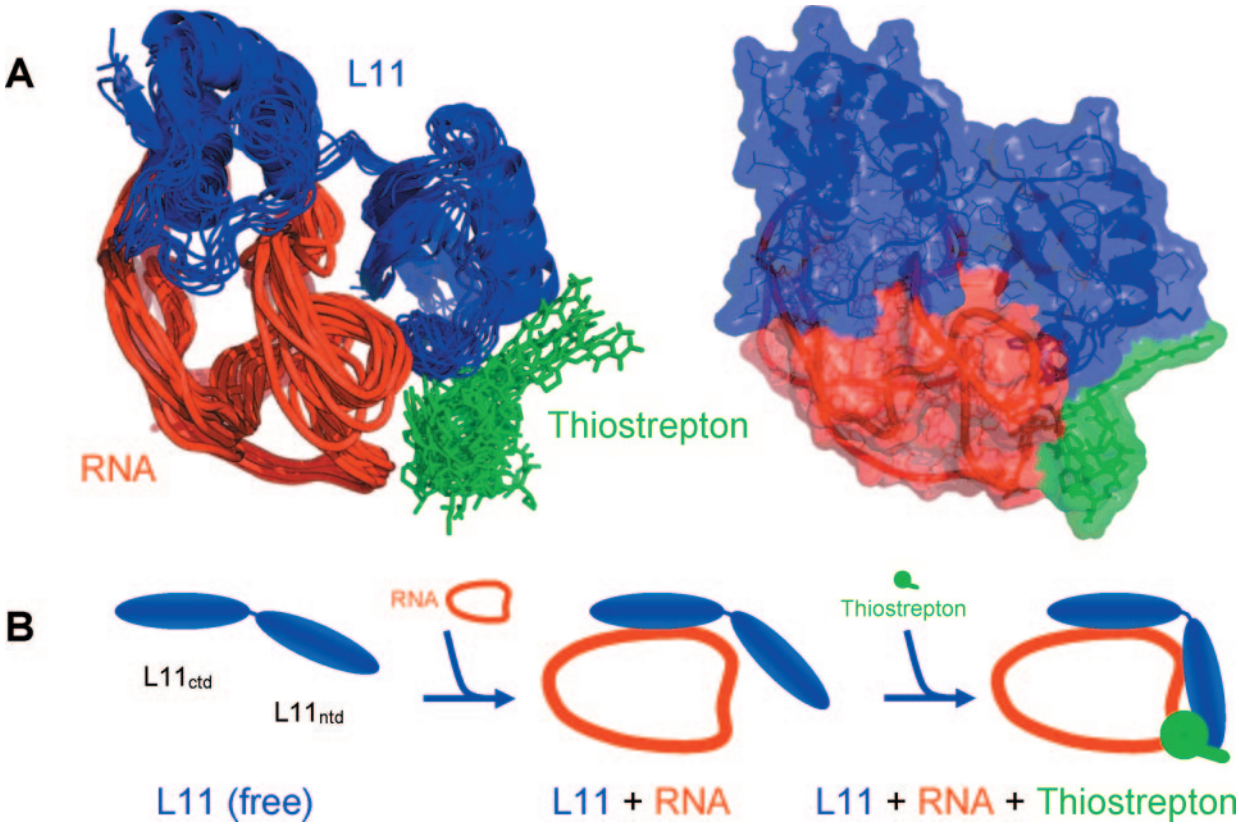

Figure 7. (**A**) Docking results of L11–RNA–thiostrepton. The bundle of the 10 best docking results from the top-ranked HADDOCK cluster is shown for the docking of L11 (blue), RNA (red) and thiostrepton (green) on the left. A combined ribbon/surface diagram for the best representative of the predominant docking orientation (same orientation as the bundle) is shown on the right. The side-chains of the RNA A1067, A1095 and the L11 24–36 residues are indicated by bold sticks. AIRs are defined for the interaction surface of $L11_{ctd}$ and the RNA (L11 residues: 74–76, 80, 87–94, 112, 115–119, 123, 126, 127, 130, 131, 133–135 and RNA nucleotides: 1058–1060, 1062–1065, 1075–1083 and 1088). For the binding of thiostrepton to the RNA, ambiguous restraints have been defined that are based on NOE data (53) for specific protons of the thiostrepton (thr-2, tzb-3 and tsi-4) to the H2, H8 and H1′ protons of any adenosine and cytosine within or near the binding pocket (nucleotides A:1067, 1069, 1070, 1073, 1095, 1096, 1098 and C: 1097 and 1100). Two AIRs were defined based on mutational analysis (47) for A1067 and A1095 to thiostrepton. $L11_{ntd}$ residues 11, 12, 24, 28, 29, 33, 36 and 56 have been selected as active restraints to either thiostrepton or the RNA (1059–1064, 1068–1070 and 1095–1098). Residues 9–14, 21–37, 39, 40, 53, 55–57, 74 of L11 have been defined as passive restraints for the interaction with thiostrepton. (**B**) Model for L11 binding to RNA and thiostrepton. The L11 (blue) domain orientation changes upon binding to the 23S RNA region (red) and the thiostrepton antibiotic (green). The interaction specifically influences the dynamical properties of both domains.

RNA stem–loops and the first helix of $L11_{ntd}$. Many contacts are observed for the tzo-1, thr-2, tzb-3 and tsi-4 residues of the thiazoline-macrocycle to the A1067 and A1095 nt of the RNA and to the P26, G29 and Q30 residues of the L11 protein. For the dehydroalanine tail, contacts are observed to the I35 and M36 residues of the L11 protein. Furthermore, the model explains that other CSPs observed in $L11_{ntd}$ upon binding to thiostrepton are caused by moving $L11_{ntd}$ closer to the RNA (residues 11, 12 and 56). The quinaldic-acid-macrocycle is mostly located on the outside and does not seem to make many significant contacts to either the RNA and the L11 protein except for qua-7 and ala-11 which are still relatively near to the RNA A1095 and residues G29 and Q30 of the L11 protein. Since the other members of the thiazole family of antibiotics as micrococcin and siomycin differ mainly in this quinaldic-acid-macrocycle, a similar binding mode may be expected. This will present dissimilar surfaces to the outside which may differentially influence the interactions with other factors and RNA.

The buried surface area between the L11 and RNA in the ternary complex is 3300 $Å^2$, which is substantially larger than the surface area buried in the L11–RNA complex. [2700 $Å^2$ for 1MMS (26)]. The interface is also much larger than for the average protein–RNA complex (1130 ± 550 $Å^2$) (87). In addition, the thiostrepton antibiotic itself buries another 880 $Å^2$ of the surface area. These large changes in the buried surface areas correlate well with the high-binding affinity of thiostrepton (22,46).

DISCUSSION AND CONCLUSION

The $L11_{ntd}$ and $L11_{ctd}$ are connected by a short linker containing two prolines which limits the conformational space. Nevertheless distinctly different domain orientations were observed when aligning the free form L11 structure with the X-ray structures of the L11–RNA complex (36). Analysis of various X-ray and cryo-EM structures containing L11 and

its cognate RNA indicated that there are considerable differences in the relative orientation of $L11_{ntd}$ with respect to $L11_{ctd}$ and the RNA (Figure 4).

We have assigned the NMR backbone resonances of L11 in the binary complex with its cognate RNA and in the ternary complex with the RNA and thiostrepton in order to map the binding surface of L11 for the RNA and the antibiotic (Figures 2 and 3). The RNA-binding site is located in the $L11_{ctd}$, which is in good agreement with the X-ray structure of the complex (26). Furthermore, the HetNOE, T_2 relaxation data and the order parameters (S^2) indicate a rigidification of the flexible loop region (residues 86–96) in this domain. The loop undergoes an induced fit conformational change and makes a significant number of hydrogen bond contacts and salt-bridges to the RNA as evident from the X-ray structure (26). Only relatively small CSPs are found in $L11_{ntd}$. Together with the relatively smaller T_1 relaxation observed for $L11_{ntd}$ (Figure 5) in comparison with $L11_{ctd}$, it indicates more freedom and flexibility for the entire N-terminal domain, which is in agreement with the observed different possible orientations of this domain. Addition of thiostrepton caused a further reduction of flexibility in $L11_{ntd}$ to the same magnitude as for $L11_{ctd}$ indicating a more rigid structure for the ternary complex. The thiostrepton mainly introduced CSPs in $L11_{ntd}$, which is in agreement with the binding site as indicated by Lentzen *et al*. (53). Thiostrepton-resistant mutations at conserved positions in $L11_{ntd}$ (prolines 22, 23 and 26) have been reported before (50,52). These proline sites cannot be mapped with our amide CSPs, but are clearly within the binding area. The CSPs observed upon binding to thiostrepton were considerably smaller (Figure 2B) in comparison with the ones observed upon binding to the RNA. This indicates that no severe structural changes occur after binding of the antibiotic. The relative orientation of both L11 domains has been determined using RDC data for the binary and ternary complex and before (36) for the free form of L11 (Figure 6). It is evident from the conformational and dynamics data that a domain rearrangement occurs upon binding to the RNA and thiostrepton which places $L11_{ntd}$ closer to the RNA. The RNA-bound orientation of L11 mostly resembles a functional state in which it is able to bind to the elongations factors EF-G and EF-Tu. However, upon binding to the thiostrepton antibiotic, $L11_{ntd}$ rotates to an inhibitory state, which prevents elongation factor binding and possibly also affects release factor binding.

The thiostrepton binding model proposed by Lentzen *et al*. (53) was only based on intermolecular NOEs between thiostrepton and the free RNA. A major limitation of this model is that the L11 protein was not part of the study and the docking was performed using a rigid body model of the L11–RNA complex (26), rather than considering the possibility of multiple conformations in the binary complex. From our study it is evident that the domain orientation of L11 does not remain the same for the binary and ternary complex. Therefore, we have calculated the structure of the ternary complex using additional conformational and interaction data for the L11 protein (Figure 7A). The structure of the thiostrepton remains a weakness in our model as we also started from the known X-ray structure of the antibiotic in isolation (78). We reduced this limitation to some extent by leaving its structure flexible during all stages of the docking calculation. Due to the intermolecular NOEs observed for the thiostrepton thr-2 side-chain to the RNA (53), which is positioned, inside the antibiotic, according to the X-ray structure (78), it is a very realistic assumption that the conformation will change upon interaction.

The presented docking model of the ternary complex shows a preferential binding of the antibiotic underneath $L11_{ntd}$ and next to the RNA stemloops containing A1067 and A1095. The model is well in agreement with biochemical and NMR interaction data. The position of the thiazoline macrocylce relative to the RNA is rather comparable with the model from Lentzen *et al*. (53), but shifted to some extent in the direction of the stem–loop containing A1095. In contrast, as a result of our additional data for the L11 protein and the included flexibility for the interaction sites and the thiostrepton antibiotic, the positions and orientations of the dehydroalanine tail and the $L11_{ntd}$ are different. Our model indicates that the L11–RNA–thiostrepton ternary complex is very compact as the $L11_{ntd}$ is positioned closely to the RNA, which is stabilized by the antibiotic. The thiostrepton-resistant mutations (prolines 22, 23 and 26) in $L11_{ntd}$ (50,52) are in close proximity of the thiazoline macrocylce of thiostrepton as well as the RNA loop containing A1067. The mutations alleviate the functional effects without affecting the binding affinity of the antibiotic with the RNA. It is suggested that they counteract the stabilization of the complex by destabilizing the L11ntd region, which allows the protein domain to move despite the presence of the antibiotic. This is well in agreement with the location of these residues in our model of the ternary complex.

The model of the ternary L11–RNA–thiostrepton complex indicates that the quinaldic-acid macrocycle is mostly at the outside of the complex. Only for the residues qua-7 and ala-11, contacts are observed to the RNA A1095 and the L11 protein. Another thiazole antibiotic, nosiheptide, connects a second macrocyle from xaa-6 to tsi-4. The quinaldic acid is replaced by an indole moiety at nearly the same position as qua-7; which slightly influences the interaction with the RNA (53). The micrococcin antibiotic misses the second macrocyle completely and therefore the additional stabilizing interactions of the qua-7 (and ala-11), which could explain the different binding mode of this antibiotic (53). Furthermore the dehydroalanine tail for thiostrepton, the nosiheptide and micrococcin are slightly different, which may influence the interaction with L11 and therefore the orientation of $L11_{ntd}$. In addition there is a large difference in the tsi-4 side-chain of the thiazoline-macrocycle for micrococcin. Lentzen *et al*. (53) found specific NOE contacts from this sidechain to the RNA. As this part is reduced in micrococcin it may influence the way of binding and/or the binding affinity. Either changes in the dehydroalanine tail, the missing quinaldic acid macrocyle and changes in the tsi-4 for micrococcin may give rise to a different binding mode and affinity. As this may cause an more open and less tight complex, it could explain the differences observed in protection of the RNA (47,53). The variation on the outside of the complex may additionally have a specific influence on the binding of other factors, (such as EF-G, EF-Tu, RF-1 and RF-2).

Although 23S RNA is essential for binding of thiostrepton, the L11 protein appears to be important for its inhibitory mechanism. It has been shown that in ribosomes that lack

L11, the sensitivity to thiostrepton is greatly reduced (88). The L11 protein enhances the thiostrepton binding by a factor of 100–1000 (54,55). From this data, tight binding of the L11–RNA region to thiostrepton would be expected, which supports the complex as proposed here (Figure 7A). Furthermore, the total buried surface area in the ternary complex of nearly 4200 $Å^2$ is much larger than for the L11–RNA binary complex (26), explaining the high-binding affinity of thiostrepton (22,46).

In conclusion, thiostrepton stabilizes and enlarges the binding interface between L11 and the 23S rRNA in such a tight manner that it prevents the $L11_{ntd}$ from structural transitions to other orientations, such as the EF-G bound. The N-terminal domain of L11 is accordingly trapped into a rigid (inhibitory) state (Figure 7B), which has a dramatic effect on the level of protein synthesis by the ribosome. In general, our findings show how various (small) components within the ribosomal machinery can have a drastic impact on the overall functionality.

SUPPLEMENTARY DATA

Supplementary Data are available at NAR online.

ACCESSION NUMBERS

Coordinates for the model of the ternary complex have been deposited in the Protein Data Bank (PDB, ID code 2NYO). The chemical shift values and RDCs have been deposited in the Biological Magnetic Resonance data Bank (BMRB, ID codes 7307 and 7308).

ACKNOWLEDGEMENTS

The authors thank Alexandre Bonvin for providing the multi-component docking version of HADDOCK. The work was supported by DFG (Sonderforschungsbereich 579), the SPINE project of the European commission and the state of Hesse (BMRZ). Funding to pay the Open Access publication charges for this article was provided by SFB 579.

Conflict of interest statement. None declared.

REFERENCES

1. Ban,N., Nissen,P., Hansen,J., Moore,P.B. and Steitz,T.A. (2000) The complete atomic structure of the large ribosomal subunit at 2.4 A resolution. *Science*, **289**, 905–920.
2. Schlünzen,F., Tocilj,A., Zarivach,R., Harms,J., Glühmann,M., Janell,D., Bashan,A., Bartels,H., Agmon,I., Franceschi,F. *et al*. (2000) Structure of functionally activated small ribosomal subunit at 3.3 angstroms resolution. *Cell*, **102**, 615–623.
3. Wimberly,B.T., Brodersen,D.E., Clemons,W.M.,Jr, Morgan-Warren,R.J., Carter,A.P., Vonrhein,C., Hartsch,T. and Ramakrishnan,V. (2000) Structure of the 30S ribosomal subunit. *Nature*, **407**, 327–339.
4. Yusupov,M.M., Yusupova,G.Z., Baucom,A., Lieberman,K., Earnest,T.N., Cate,J.H. and Noller,H.F. (2001) Crystal structure of the ribosome at 5.5 A resolution. *Science*, **292**, 883–896.
5. Harms,J., Schlünzen,F., Zarivach,R., Bashan,A., Gat,S., Agmon,I., Bartels,H., Franceschi,F. and Yonath,A. (2001) High resolution structure of the large ribosomal subunit from a mesophilic eubacterium. *Cell*, **107**, 679–688.
6. Schuwirth,B.S., Borovinskaya,M.A., Hau,C.W., Zhang,W., Vila-Sanjurjo,A., Holton,J.M. and Cate,J.H. (2005) Structures of the bacterial ribosome at 3.5 A resolution. *Science*, **310**, 827–834.
7. Agrawal,R.K., Heagle,A.B., Penczek,P., Grassucci,R.A. and Frank,J. (1999) EF-G-dependent GTP hydrolysis induces translocation accompanied by large conformational changes in the 70S ribosome. *Nature Struct. Biol*., **6**, 643–647.
8. Frank,J. and Agrawal,R.K. (2000) A ratchet-like inter-subunit reorganization of the ribosome during translocation. *Nature*, **406**, 318–322.
9. Stark,H., Rodnina,M.V., Wieden,H.J., van Heel,M. and Wintermeyer,W. (2000) Large-scale movement of elongation factor G and extensive conformational change of the ribosome during translocation. *Cell*, **100**, 301–309.
10. Brodersen,D.E., Clemons,W.M.,Jr, Carter,A.P., Morgan-Warren,R.J., Wimberly,B.T. and Ramakrishnan,V. (2000) The structural basis for the action of the antibiotics tetracycline, pactamycin, and hygromycin B on the 30S ribosomal subunit. *Cell*, **103**, 1143–1154.
11. Ogle,J.M., Brodersen,D.E., Clemons,W.M.,Jr, Tarry,M.J., Carter,A.P. and Ramakrishnan,V. (2001) Recognition of cognate transfer RNA by the 30S ribosomal subunit. *Science*, **292**, 897–902.
12. Pioletti,M., Schlunzen,F., Harms,J., Zarivach,R., Gluhmann,M., Avila,H., Bashan,A., Bartels,H., Auerbach,T., Jacobi,C. *et al*. (2001) Crystal structures of complexes of the small ribosomal subunit with tetracycline, edeine and IF3. *EMBO J*., **20**, 1829–1839.
13. Yusupova,G.Z., Yusupov,M.M., Cate,J.H. and Noller,H.F. (2001) The path of messenger RNA through the ribosome. *Cell*, **106**, 233–241.
14. Ogle,J.M., Murphy,F.V., Tarry,M.J. and Ramakrishnan,V. (2002) Selection of tRNA by the ribosome requires a transition from an open to a closed form. *Cell*, **111**, 721–732.
15. Schmeing,T.M., Seila,A.C., Hansen,J.L., Freeborn,B., Soukup,J.K., Scaringe,S.A., Strobel,S.A., Moore,P.B. and Steitz,T.A. (2002) A pre-translocational intermediate in protein synthesis observed in crystals of enzymatically active 50S subunits. *Nature Struct. Biol*., **9**, 225–230.
16. Hansen,J.L., Ippolito,J.A., Ban,N., Nissen,P., Moore,P.B. and Steitz,T.A. (2002) The structures of four macrolide antibiotics bound to the large ribosomal subunit. *Mol. Cell*, **10**, 117–128.
17. Gao,H., Sengupta,J., Valle,M., Korostelev,A., Eswar,N., Stagg,S.M., Van Roey,P., Agrawal,R.K., Harvey,S.C., Sali,A. *et al*. (2003) Study of the structural dynamics of the *E.coli* 70S ribosome using real-space refinement. *Cell*, **113**, 789–801.
18. Schmeing,T.M., Moore,P.B. and Steitz,T.A. (2003) Structures of deacylated tRNA mimics bound to the E site of the large ribosomal subunit. *RNA*, **9**, 1345–1352.
19. Petry,S., Brodersen,D.E., Murphy,F.V.,IV, Dunham,C.M., Selmer,M., Tarry,M.J., Kelley,A.C. and Ramakrishnan,V. (2005) Crystal structures of the ribosome in complex with release factors RF1 and RF2 bound to a cognate stop codon. *Cell*, **123**, 1255–1266.
20. Jenner,L., Romby,P., Rees,B., Schulze-Briese,C., Springer,M., Ehresmann,C., Ehresmann,B., Moras,D., Yusupova,G. and Yusupov,M. (2005) Translational operator of mRNA on the ribosome: how repressor proteins exclude ribosome binding. *Science*, **308**, 120–123.
21. Korostelev,A., Trakhanov,S., Laurberg,M. and Noller,H.F. (2006) Crystal structure of a 70S ribosome-tRNA complex reveals functional interactions and rearrangements. *Cell*, **126**, 1065–1077.
22. Thompson,J., Cundliffe,E. and Stark,M. (1979) Binding of thiostrepton to a complex of 23-S rRNA with ribosomal protein L11. *Eur. J. Biochem*., **98**, 261–265.
23. Schmidt,F.J., Thompson,J., Lee,K., Dijk,J. and Cundliffe,E. (1981) The binding site for ribosomal protein L11 within 23 S ribosomal RNA of *Escherichia coli*. *J. Biol. Chem*., **256**, 12301–12305.
24. Tate,W.P., Dognin,M.J., Noah,M., Stoffler-Meilicke,M. and Stoffler,G. (1984) The NH2-terminal domain of *Escherichia coli* ribosomal protein L11. Its three-dimensional location and its role in the binding of release factors 1 and 2. *J. Biol. Chem*., **259**, 7317–7324.
25. Stark,M.J. and Cundliffe,E. (1979) Requirement for ribosomal protein BM-L11 in stringent control of RNA synthesis in *Bacillus megaterium*. *Eur. J. Biochem*., **102**, 101–105.
26. Wimberly,B.T., Guymon,R., McCutcheon,J.P., White,S.W. and Ramakrishnan,V. (1999) A detailed view of a ribosomal active site: the structure of the L11–RNA complex. *Cell*, **97**, 491–502.

27. Conn,G.L., Draper,D.E., Lattman,E.E. and Gittis,A.G. (1999) Crystal structure of a conserved ribosomal protein–RNA complex. *Science*, **284**, 1171–1174.
28. Conn,G.L., Gittis,A.G., Lattman,E.E., Misra,V.K. and Draper,D.E. (2002) A compact RNA tertiary structure contains a buried backbone-K+ complex. *J. Mol. Biol.*, **318**, 963–973.
29. Bukhman,Y.V. and Draper,D.E. (1997) Affinities and selectivities of divalent cation binding sites within an RNA tertiary structure. *J. Mol. Biol.*, **273**, 1020–1031.
30. Shiman,R. and Draper,D.E. (2000) Stabilization of RNA tertiary structure by monovalent cations. *J. Mol. Biol.*, **302**, 79–91.
31. Draper,D.E. and Xing,Y. (1995) Protein recognition of a ribosomal RNA tertiary structure. *Nucleic Acids Symp. Ser.*, **33**, 5–7.
32. Xing,Y. and Draper,D.E. (1995) Stabilization of a ribosomal RNA tertiary structure by ribosomal protein L11. *J. Mol. Biol.*, **249**, 319–331.
33. Blyn,L.B., Risen,L.M., Griffey,R.H. and Draper,D.E. (2000) The RNA-binding domain of ribosomal protein L11 recognizes an rRNA tertiary structure stabilized by both thiostrepton and magnesium ion. *Nucleic Acids Res.*, **28**, 1778–1784.
34. Xing,Y., Guha Thakurta,D. and Draper,D.E. (1997) The RNA binding domain of ribosomal protein L11 is structurally similar to homeodomains. *Nature Struct. Biol.*, **4**, 24–27.
35. Markus,M.A., Hinck,A.P., Huang,S., Draper,D.E. and Torchia,D.A. (1997) High resolution solution structure of ribosomal protein L11-C76, a helical protein with a flexible loop that becomes structured upon binding to RNA. *Nature Struct. Biol.*, **4**, 70–77.
36. Ilin,S., Hoskins,A., Ohlenschläger,O., Jonker,H.R.A., Schwalbe,H. and Wöhnert,J. (2005) Domain reorientation and induced fit upon RNA binding: solution structure and dynamics of ribosomal protein L11 from *Thermotoga maritima*. *Chembiochem*, **6**, 1611–1618.
37. Hinck,A.P., Markus,M.A., Huang,S., Grzesiek,S., Kustonovich,I., Draper,D.E. and Torchia,D.A. (1997) The RNA binding domain of ribosomal protein L11: three-dimensional structure of the RNA-bound form of the protein and its interaction with 23 S rRNA. *J. Mol. Biol.*, **274**, 101–113.
38. Agrawal,R.K., Linde,J., Sengupta,J., Nierhaus,K.H. and Frank,J. (2001) Localization of L11 protein on the ribosome and elucidation of its involvement in EF-G-dependent translocation. *J. Mol. Biol.*, **311**, 777–787.
39. Valle,M., Zavialov,A., Li,W., Stagg,S.M., Sengupta,J., Nielsen,R.C., Nissen,P., Harvey,S.C., Ehrenberg,M. and Frank,J. (2003) Incorporation of aminoacyl-tRNA into the ribosome as seen by cryo-electron microscopy. *Nature Struct. Biol.*, **10**, 899–906.
40. Pestka,S. (1970) Thiostrepton: a ribosomal inhibitor of translocation. *Biochem. Biophys. Res. Commun.*, **40**, 667–674.
41. Cundliffe,E. and Thompson,J. (1981) Concerning the mode of action of micrococcin upon bacterial protein synthesis. *Eur. J. Biochem.*, **118**, 47–52.
42. Brot,N., Tate,W.P., Caskey,C.T. and Weissbach,H. (1974) The requirement for ribosomal proteins L7 and L12 in peptide-chain termination. *Proc. Natl Acad. Sci. USA*, **71**, 89–92.
43. Cameron,D.M., Thompson,J., March,P.E. and Dahlberg,A.E. (2002) Initiation factor IF2, thiostrepton and micrococcin prevent the binding of elongation factor G to the *Escherichia coli* ribosome. *J. Mol. Biol.*, **319**, 27–35.
44. Rodnina,M.V., Savelsbergh,A., Matassova,N.B., Katunin,V.I., Semenkov,Y.P. and Wintermeyer,W. (1999) Thiostrepton inhibits the turnover but not the GTPase of elongation factor G on the ribosome. *Proc. Natl. Acad. Sci. USA*, **96**, 9586–9590.
45. Egebjerg,J., Douthwaite,S. and Garrett,R.A. (1989) Antibiotic interactions at the GTPase-associated centre within *Escherichia coli* 23S rRNA. *EMBO J.*, **8**, 607–611.
46. Thompson,J. and Cundliffe,E. (1991) The binding of thiostrepton to 23S ribosomal RNA. *Biochimie*, **73**, 1131–1135.
47. Rosendahl,G. and Douthwaite,S. (1994) The antibiotics micrococcin and thiostrepton interact directly with 23S rRNA nucleotides 1067A and 1095A. *Nucleic Acids Res.*, **22**, 357–363.
48. Bowen,W.S., Van Dyke,N., Murgola,E.J., Lodmell,J.S. and Hill,W.E. (2005) Interaction of thiostrepton and elongation factor-G with the ribosomal protein L11-binding domain. *J. Biol. Chem.*, **280**, 2934–2943.
49. Cundliffe,E. (1986) Involvement of specific portions of rRNA in defined ribosomal functions: a study utilizing antibiotics. In Hardesty,B. and Kramer,G. (eds), *Structure, Function and Genetics of Ribosomes*. Springer-Verlag, NY, pp. 586–604.
50. Porse,B.T., Leviev,I., Mankin,A.S. and Garrett,R.A. (1998) The antibiotic thiostrepton inhibits a functional transition within protein L11 at the ribosomal GTPase centre. *J. Mol. Biol.*, **276**, 391–404.
51. Porse,B.T., Cundliffe,E. and Garrett,R.A. (1999) The antibiotic micrococcin acts on protein L11 at the ribosomal GTPase centre. *J. Mol. Biol.*, **287**, 33–45.
52. Cameron,D.M., Thompson,J., Gregory,S.T., March,P.E. and Dahlberg,A.E. (2004) Thiostrepton-resistant mutants of *Thermus thermophilus*. *Nucleic Acids Res.*, **32**, 3220–3227.
53. Lentzen,G., Klinck,R., Matassova,N., Aboul-ela,F. and Murchie,A.I. (2003) Structural basis for contrasting activities of ribosome binding thiazole antibiotics. *Chem. Biol.*, **10**, 769–778.
54. Xing,Y. and Draper,D.E. (1996) Cooperative interactions of RNA and thiostrepton antibiotic with two domains of ribosomal protein L11. *Biochemistry*, **35**, 1581–1588.
55. Bausch,S.L., Poliakova,E. and Draper,D.E. (2005) Interactions of the N-terminal domain of ribosomal protein L11 with thiostrepton and rRNA. *J. Biol. Chem.*, **280**, 29956–29963.
56. Dominguez,C., Boelens,R. and Bonvin,A.M. (2003) HADDOCK: a protein-protein docking approach based on biochemical or biophysical information. *J. Am. Chem. Soc.*, **125**, 1731–1737.
57. Gutell,R.R., Gray,M.W. and Schnare,M.N. (1993) A compilation of large subunit (23S and 23S-like) ribosomal RNA structures: 1993. *Nucleic Acids Res.*, **21**, 3055–3074.
58. Lu,M. and Draper,D.E. (1994) Bases defining an ammonium and magnesium ion-dependent tertiary structure within the large subunit ribosomal RNA. *J. Mol. Biol.*, **244**, 572–585.
59. Wyatt,J.R., Chastain,M. and Puglisi,J.D. (1991) Synthesis and purification of large amounts of RNA oligonucleotides. *Biotechniques*, **11**, 764–769.
60. Cavanagh,J., Fairbrother,W.J., Palmer,A.G.,III and Skelton,N.J. (1996) *Protein NMR Spectroscopy—Principles and Practice*. Academic Press, San Diego, CA.
61. Delaglio,F., Grzesiek,S., Vuister,G.W., Zhu,G., Pfeifer,J. and Bax,A. (1995) NMRPipe: a multidimensional spectral processing system based on UNIX pipes. *J. Biomol. NMR*, **6**, 277–293.
62. Ilin,S., Hoskins,A., Schwalbe,H. and Wöhnert,J. (2003) NMR assignment of the full-length ribosomal protein L11 from *Thermotoga maritima*. *J. Biomol. NMR*, **25**, 163–164.
63. Wang,Y.X., Marquardt,J.L., Wingfield,P., Stahl,S.J., Lee-Huang,S., Torchia,D. and Bax,A. (1998) Simultaneous measurement of 1H-15N, 1H-13C', and 15N-13C' dipolar couplings in a perdeuterated 30 kDa protein dissolved in a dilute liquid crystalline phase. *J. Am. Chem. Soc.*, **120**, 7385–7386.
64. Ottiger,M., Delaglio,F. and Bax,A. (1998) Measurement of J and dipolar couplings from simplified two-dimensional NMR spectra. *J. Magn. Reson.*, **131**, 373–378.
65. Dosset,P., Hus,J.C., Marion,D. and Blackledge,M. (2001) A novel interactive tool for rigid-body modeling of multi-domain macromolecules using residual dipolar couplings. *J. Biomol. NMR*, **20**, 223–231.
66. Zweckstetter,M. and Bax,A. (2000) Prediction of sterically induced alignment in a dilute liquid crystalline phase: aid to protein structure determination by NMR. *J. Am. Chem. Soc.*, **122**, 3791–3792.
67. Kay,L.E., Nicholson,L.K., Delaglio,F., Bax,A. and Torchia,D.A. (1992) Pulse sequences for removal of the effects of cross correlation between dipolar and chemical-shift anisotropy relaxation mechanisms on the measurement of heteronuclear T1 and T2 values in proteins. *J. Magn. Reson.*, **97**, 359–375.
68. Farrow,N.A., Muhandiram,R., Singer,A.U., Pascal,S.M., Kay,C.M., Gish,G., Shoelson,S.E., Pawson,T., Forman-Kay,J.D. and Kay,L.E. (1994) Backbone dynamics of a free and phosphopeptide-complexed Src homology 2 domain studied by 15N NMR relaxation. *Biochemistry*, **33**, 5984–6003.
69. Dayie,K.T. and Wagner,G. (1994) Relaxation-rate measurements for 15N-1H groups with pulsed-field gradients and preservation of coherence pathways. *J. Magn. Reson. A*, **111**, 121–126.
70. Dosset,P., Hus,J.C., Blackledge,M. and Marion,D. (2000) Efficient analysis of macromolecular rotational diffusion from heteronuclear relaxation data. *J. Biomol. NMR*, **16**, 23–28.
71. Lipari,G. and Szabo,A. (1982) Model-free approach to the interpretation of nuclear magnetic resonance relaxation in

macromolecules. 2. Analysis of experimental results. *J. Am. Chem. Soc*., **104**, 4559–4570.
72. Lipari,G. and Szabo,A. (1982) Model-free approach to the interpretation of nuclear magnetic resonance relaxation in macromolecules. 1. Theory and range of validity. *J. Am. Chem. Soc*., **104**, 4546–4559.
73. Garcia de la Torre,J., Huertas,M.L. and Carrasco,B. (2000) HYDRONMR: prediction of NMR relaxation of globular proteins from atomic-level structures and hydrodynamic calculations. *J. Magn. Reson*., **147**, 138–146.
74. Brunger,A.T., Adams,P.D., Clore,G.M., DeLano,W.L., Gros,P., Grosse-Kunstleve,R.W., Jiang,J.S., Kuszewski,J., Nilges,M., Pannu,N.S. *et al*. (1998) Crystallography & NMR system: a new software suite for macromolecular structure determination. *Acta Crystallogr. D. Biol. Crystallogr*., **54**, 905–921.
75. Linge,J.P. and Nilges,M. (1999) Influence of non-bonded parameters on the quality of NMR structures: a new force field for NMR structure calculation. *J. Biomol. NMR*, **13**, 51–59.
76. Moglich,A., Weinfurtner,D., Gronwald,W., Maurer,T. and Kalbitzer,H.R. (2005) PERMOL: restraint-based protein homology modeling using DYANA or CNS. *Bioinformatics*, **21**, 2110–2111.
77. Ye,K., Serganov,A., Hu,W., Garber,M. and Patel,D.J. (2002) Ribosome-associated factor Y adopts a fold resembling a double-stranded RNA binding domain scaffold. *Eur. J. Biochem*., **269**, 5182–5191.
78. Bond,C.S., Shaw,M.P., Alphey,M.S. and Hunter,W.N. (2001) Structure of the macrocycle thiostrepton solved using the anomalous dispersion contribution of sulfur. *Acta Crystallogr. D. Biol. Crystallogr*., **57**, 755–758.
79. Parkinson,G., Vojtechovsky,J., Clowney,L., Brunger,A.T. and Berman,H.M. (1996) New parameters for the refinement of nucleic acid-containing structures. *Acta Crystallogr. D. Biol. Crystallogr*., **52**, 57–64.
80. Schuttelkopf,A.W. and van Aalten,D.M. (2004) PRODRG: a tool for high-throughput crystallography of protein-ligand complexes. *Acta Crystallogr. D. Biol. Crystallogr*., **60**, 1355–1363.
81. Williamson,J.R. (2000) Induced fit in RNA-protein recognition. *Nature Struct. Biol*., **7**, 834–837.
82. Mueller,F., Sommer,I., Baranov,P., Matadeen,R., Stoldt,M., Wöhnert,J., Görlach,M., van Heel,M. and Brimacombe,R. (2000) The 3D arrangement of the 23 S and 5 S rRNA in the *Escherichia coli* 50 S ribosomal subunit based on a cryo-electron microscopic reconstruction at 7.5 A resolution. *J. Mol. Biol*., **298**, 35–59.
83. Schlünzen,F., Harms,J.M., Franceschi,F., Hansen,H.A., Bartels,H., Zarivach,R. and Yonath,A. (2003) Structural basis for the antibiotic activity of ketolides and azalides. *Structure*, **11**, 329–338.
84. Harms,J.M., Schlunzen,F., Fucini,P., Bartels,H. and Yonath,A. (2004) Alterations at the peptidyl transferase centre of the ribosome induced by the synergistic action of the streptogramins dalfopristin and quinupristin. *BMC Biol*., **2**, 4.
85. Vila-Sanjurjo,A., Ridgeway,W.K., Seymaner,V., Zhang,W., Santoso,S., Yu,K. and Cate,J.H. (2003) X-ray crystal structures of the WT and a hyper-accurate ribosome from *Escherichia coli*. *Proc. Natl Acad. Sci. USA*, **100**, 8682–8687.
86. Vila-Sanjurjo,A., Schuwirth,B.S., Hau,C.W. and Cate,J.H. (2004) Structural basis for the control of translation initiation during stress. *Nature Struct. Mol. Biol*., **11**, 1054–1059.
87. Jones,S., Daley,D.T., Luscombe,N.M., Berman,H.M. and Thornton,J.M. (2001) Protein–RNA interactions: a structural analysis. *Nucleic Acids Res*., **29**, 943–954.
88. Cundliffe,E., Dixon,P., Stark,M., Stoffler,G., Ehrlich,R., Stoffler-Meilicke,M. and Cannon,M. (1979) Ribosomes in thiostrepton-resistant mutants of *Bacillus megaterium* lacking a single 50 S subunit protein. *J. Mol. Biol*., **132**, 235–252.